Supporting information

Adsorption–catalysis integrated Au@ZIF-8 for structural detoxification and trace detection of nitro impurities

Congyu Ma[#,a,b], Suhang Hu[#,b], Yutong Xiao[b], Xueying Wang[b], Feng Zheng[*,b], Wenyuan Liu[*,b,c], Lingfei Han[*,b,c]

[a] Jiangsu Institute for Drug Control, Nanjing 210019, China.

[b] Department of Pharmaceutical Analysis, China Pharmaceutical University, Nanjing 211198, China

[c] Zhejiang Center for Safety Study of Drug Substances (Industrial Technology Innovation Platform), Hangzhou 310018, China

*E-mail: liuwenyuan@cpu.edu.cn (Wenyuan Liu)

*E-mail: hanlingfei@cpu.edu.cn (Lingfei Han)

Content

Methods

S1. Materials Instruments

Zinc nitrate hexahydrate ($Zn(NO_3)_2 \cdot 6H_2O$, ≥99%, AR), trisodium citrate ($C_6H_5Na_3O_7$, AR) and 4-nitrophenol (4-NP, AR) were purchased from Nanjing Chemical Reagent Co., Ltd. (China). Dimethylimidazole (2-MIM, 98%) and valsartan (HPLC Grade) were purchased from Aladdin Biochemical Technology Co., Ltd. (Shanghai, China). Tetrachloroauric acid ($HAuCl_4$, 99%) was purchased from Tianjin Heowns Biochemical Technology Co., Ltd. (China). Sodium borohydride ($NaBH_4$, ≥96.0%, AR) was purchased from Sinopharm Chemical Reagent Co., Ltd. (China). *N*-nitrosodimethylamine (NDMA, 99%) was purchased from Shanghai Macklin Biochemical Co., Ltd. (Shanghai, China)). Methanol (HPLC Grade) was purchased from Merck KGaA. Ultrapure water (resistivity: 18.25 MΩ cm at 25 °C) was used in all experiments.

S2. Preparation of ZIF-8 and Au@ZIF-8

The preparation scheme of ZIF-8 is based on existing research and has been appropriately modified[1]. At room temperature (25℃), 255.0 mg of zinc nitrate hexahydrate and 4926.1 mg of 2-methylimidazole were dissolved in 12 mL of ultrapure water respectively, then slowly pour the 2-methylimidazole solution into the zinc nitrate hexahydrate solution. Stir the mixed solution thoroughly at room temperature for 24 hours. Centrifuge the resulting product at a speed of 9000 rpm/min for 10 minutes, discard the supernatant, and dissolve and disperse the lower precipitate in ultrapure water again. Repeat the centrifugation and washing steps three times, then place the precipitate in a 60℃ oven and dry overnight to obtain ZIF-8 powder.

The preparation scheme of Au@ZIF-8 was designed inspired by existing research[2]. Take 10 mg of ZIF-8 and disperse it in 5 mL of ultrapure water. Slowly add 3 mL of 0.5 mg/mL tetrachloroauric acid solution under magnetic stirring at a speed of 900 rpm/min. After thoroughly mixing with ZIF-8 solution, slowly add 200 μL of 1 mg/mL sodium borohydride solution and 4 mL of 2.5 mg/mL trisodium citrate solution. After reacting the above mixed solution at room temperature for 1 hour, centrifuge at a speed

of 9000 rpm/min for 10 minutes, discard the supernatant, and re disperse the lower precipitate with solvent. Repeat the centrifugation and washing steps three times, then place the precipitate in a 60 ℃ oven to dry overnight to obtain Au@ZIF-8 powder.

S3. Characterization of ZIF-8 and Au@ZIF-8

The different properties of the synthesized ZIF-8 and Au@ZIF-8 were revealed by using a Regulus-8100 field emission scanning electron microscope (SEM), a TF-20 high-resolution transmission electron microscope and energy dispersive spectrometer (TEM-EDS), a D8 Advance X-ray diffractometer (XRD), an IS 50 Fourier transform infrared spectrometer (FT-IR), a Malven Nano ZS90 particle size and zeta potential analyzer, and a JW-BK200B specific surface area and pore size analyzer.

S4. Adsorption Performance Test

Taking 4-NP and NDMA as examples, the adsorption performance of Au@ZIF-8 was investigated. The specific experimental procedures are as follows: Take a certain amount of Au@ZIF-8 powder and put it into 30 mL of a 4-NP solution with a certain initial mass concentration. Adjust the shaking bed temperature to 25 ℃ and oscillate at 150 rpm/min for a certain period of time. Then take the supernatant, filter it through a 0.1 μm filter, and measure the absorbance of 4-NP using a microplate reader (317 nm, Bio Tek Epoch). Measure the content of NDMA using HPLC (230 nm, Shimadzu 20AD). Calculate the adsorption amount at a certain time q_t, the adsorption amount at the equilibrium time q_e, and the removal rate R (%) according to the following formulas (1)-(3).

$$q_t = \frac{C_0 \cdot V_o - C_t \cdot V}{m}$$ Formula (1)

$$q_e = \frac{C_0 \cdot V_o - C_e \cdot V}{m}$$ Formula (2)

$$R = \frac{C_0 - C_e}{C_0} \times 100\% \quad \text{Formula (3)}$$

In the formula, C_0: initial adsorption concentration, mg/L; C_e: concentration at equilibrium adsorption time, mg/L; V_0: initial adsorption volume, L; V: volume at time t of adsorption, L; m: mass of adsorbent, g.

S4.1 Adsorption Kinetics Experiment

The adsorption kinetics of Au@ZIF-8 was studied using pseudo-first-order and pseudo-second-order kinetic models to better explain the adsorption process between the material and the substrate. The curves of adsorption capacity varying with time obtained from the experiments were nonlinearly fitted using the pseudo-first-order model in Formula (4) and the pseudo-second-order model in Formula (5).

$$\ln\left(q_e - q_t\right) = \ln q_e - k_1 t \quad \text{Formula (4)}$$

$$\frac{t}{q_t} = \frac{1}{k_2 q_e^2} + \frac{1}{q_e} t \quad \text{Formula (5)}$$

In the equation, q_e: adsorption amount at equilibrium time, mg/g; t: adsorption time, min; q_t: adsorption amount at time t, mg/g; k_1: first-order adsorption rate constant, min^{-1}; k_2: second-order adsorption rate constant, g/(mg×min).

S4.2 Adsorption isotherm experiment

By using the adsorption isotherm model to evaluate the system behavior when the adsorbate/adsorbent reach the equilibrium state, the types of interaction between Au@ZIF-8 and the adsorbate are studied. The adsorption process is explained by using the Langmuir and Freundlich equations.

$$\text{Langmuir } model: \frac{C_e}{q_e} = \frac{1}{k_L q_m} + \frac{C_e}{q_m} \quad \text{Formula (6)}$$

Freundlich model：$\ln q_e = \ln k_F + \frac{1}{n}\ln C_e$ Formula (7)

In the equation, C_e: equilibrium concentration at the equilibrium moment, mg/L; q_e: adsorption amount at the equilibrium moment, mg/g; q_m: maximum adsorption capacity, mg/g; k_L: Langmuir constant; k_F and n: Freundlich constants, representing the adsorption capacity and adsorption intensity respectively.

S5. Catalytic Performance Test

S5.1 4-NP Reduction Experiment

0.2 mL of a certain concentration of catalyst, 0.1 mL of freshly prepared 0.2 mol/L NaBH4 solution, and 5 mL of 0.1 mmol/L 4-NP solution were used. The electrons required for reduction were provided by the $NaBH_4$ solution. After the two solutions were mixed, the catalyst was added at room temperature to start the reaction. The conversion rate of 4-NP was indirectly calculated based on the change in the absorbance of the characteristic absorption peak of 4-NPi at 400 nm. The conversion rate was calculated according to formula (8). Since the borohydride sodium used in the reaction was in a significantly excessive amount, it can be assumed that its concentration remained constant throughout the entire reaction process. Therefore, this reaction can be evaluated using the pseudo-first-order kinetic equation, as shown in equations (9)-(10):

$$Conversion(\%) = \left(1 - \frac{A_t}{A_0}\right) \times 100\% \quad \text{Formula (8)}$$

$$-\frac{dC_t}{dt} = -\frac{dA_t}{dt} = k \cdot C_t = k \cdot A_t \quad \text{Formula (9)}$$

$$\ln\left(\frac{C_0}{C_t}\right) = \ln\left(\frac{A_0}{A_t}\right) = k \cdot t \quad \text{Formula (10)}$$

In the equation, Ct: the concentration at time t, mM; C0: the initial concentration, mM; At: the absorbance at 400 nm at time t; A0: the absorbance at 400 nm at the initial time;

t: the reaction time, min; k: the reaction rate constant, min^{-1}.

S5.2 NDMA catalytic derivatization method

At room temperature (25 ℃), 50 mL of ultrapure water containing 20 mg of Au@ZIF-8 catalyst was placed in a 150 mL conical flask. Before the reaction, H_2 was introduced to pre-activate the catalyst for approximately 30 minutes. Then, 20 mL of a certain concentration of NDMA solution was added under a magnetic stirring of 900 rpm/min. During the reaction, the condition of introducing H_2 was maintained, and the solution system was in a neutral environment. After 12 hours of reaction, the sample was filtered through a 0.1 μm filter membrane, resulting in the NDMA catalytic derivatization solution. It was then subjected to HPLC-MS/MS analysis (SCIEX Ttiple Quad 3500). The specific conditions are as follows.

Chromatographic system: Shimadzu LC-20AD high-performance liquid chromatography system; Chromatographic column: Agilent ZORBAX SB-C8 (4.6×250 mm, 5 μm); Mobile phase: 0.1% formic acid water (A) - methanol (B); Elution program: isocratic elution, 0-5 min, 80% B; Flow rate: 1.0 mL/min; Column temperature: 40 ℃; Injection volume: 10 μL.

Mass spectrometry conditions: Electrospray ionization source (ESI); Positive ion scanning in multiple reaction monitoring mode (MRM); Curtain gas pressure (CUR): 25 psi; Collision gas (CAD): 8 psi; Ion source temperature (TEM): 550 ℃; Nebulizing gas (GS1): 55 psi; Nebulizing gas (GS2): 55 psi; Retention time: 100 ms; Compound detection parameters: NDMA (75.05→58.05, DP: 100 V, CE: 20 eV), DMA (46.21→31.13, DP: 100 V, CE: 20 eV)

S6. DFT simulation

All configurations were calculated using the optimized Vienna Ab-initio Simulation Package[3]. The energy setting parameters are as follows: using a plane wave basis set with a cutoff of 400 eV to expand the electronic wave function; all structures were relaxed until the residual force on the free atoms was less than 0.02 eV/Å. The model selected for this study was proposed by the minimal periodic cluster of ZIF-8, and an

Au cluster containing five Au atoms was chosen as the active center, with 15 Å of vacuum area added in all three directions. Geometric optimization was performed using the Monkhorst-Pack grid in the Brillouin zone of the Gamma-type Pack k-points (Monkhorst-Pack).

For the Gibbs free energy change (ΔG) during the reaction process, this experiment used the computational hydrogen electrode (CHE) model for calculation. Additionally, the Atomic Simulation Environment (ASE) package and VESTA were used to assist in model construction and the analysis and evaluation of Bader charges, with partial charge density assessed[4,5].

S7. Ultraviolet light catalytic degradation of NDMA

This was carried out at room temperature (25°C). Two parallel groups of 30 mL NDMA (0.5 mM) solutions were prepared. One group was added with 2 mL Au@ZIF-8 (2 mg/mL) solution, and the other group was without any reagent as a blank control. The initial solution pH was adjusted to 9.5 using NaOH (0.1 M). The solution was exposed to 100 w ultraviolet light with a wavelength of 254 nm from a low-pressure mercury lamp. The photolysis began. At different time points during the reaction, 1 mL of the sample was taken, filtered through a 0.1 μm filter membrane, and analyzed using HPLC-MS/MS to determine NDMA and its degradation products.

Figures and Tables

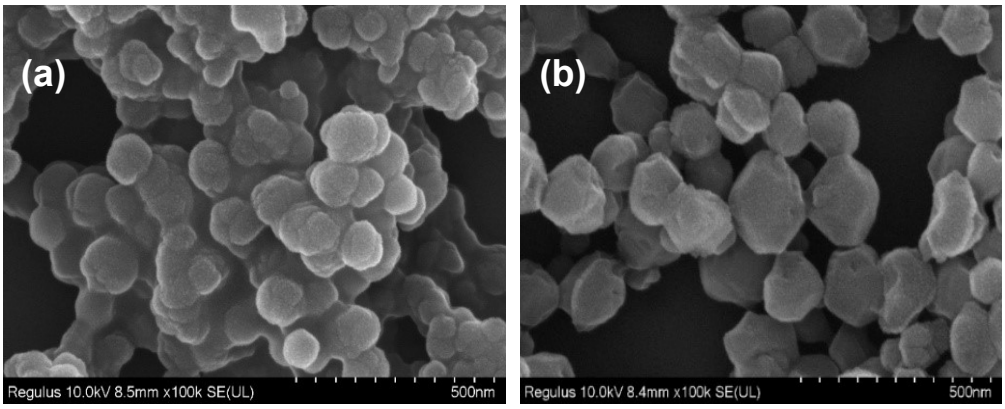

Figure S1 SEM image of ZIF-8 (a) Methanol system; (b) Ultra-pure water systems

The influence of different solvent systems on ZIF-8.

A SEM characterization comparison of different solvent systems in the preparation of ZIF-8 was established. While maintaining the unchanged ratio of zinc nitrate hexahydrate and 2-methylimidazole used in the preparation, the crystal morphology was adjusted by changing the solvent system. According to the research findings, this adjustment method would enhance the binding of imidazole to metal ions, thereby enhancing crystallization. Considering cost factors and environmental aspects, this method used green and inexpensive ultrapure water as the solvent system for the experiment, and compared the effects of the methanol system and the ultrapure water system on the synthesis of ZIF-8. The results are shown in **Figure S1**. In the methanol system, the synthesized crystals have rough surfaces and irregular shapes. Under the ultrapure water condition, the crystal structure is close to the regular dodecahedron structure. Therefore, the final reaction system for the preparation of ZIF-8 was determined to be ultrapure water.

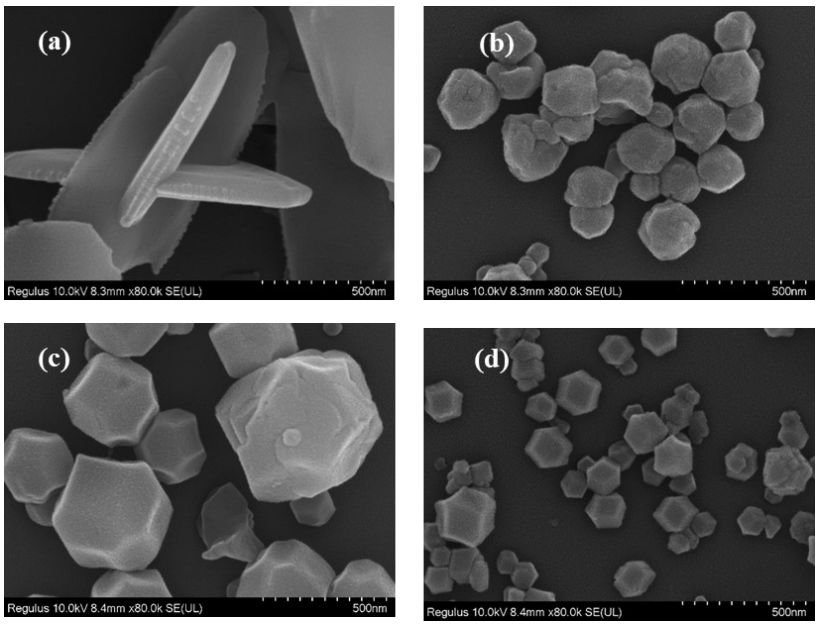

Figure S2 SEM image of Zn $(NO_3)_2$ $6H_2O$: 2-MIM at different molar ratios. (a) 1:8 (b) 1:35 (c) 1:60 (d) 1:70.

The influence of different raw material ratios on the preparation of ZIF-8.

To further improve the crystal morphology of ZIF-8, this experiment investigated the effect of different raw material ratios on the synthesis of ZIF-8. The ratios of zinc nitrate hexahydrate and 2-methylimidazole (adjusted by molar ratio) were examined as 1:8, 1:35, 1:60, and 1:70. The results are shown in **Figure S2**. It can be clearly observed that when the molar ratio is 1:70, as shown in **Figure S2c**, the prepared ZIF-8 has a smooth surface without obvious defects and presents a relatively complete rhombic dodecahedron structure. It was found that in the aqueous phase system, the traditional synthesis process often forms one-dimensional materials lacking porous structure. However, by using excessive alkaline 2-methylimidazole to deprotonate itself and the solvent system during the synthesis process, a large amount of anionic ligands are provided to accelerate the nucleation rate of ZIF-8 coordination, achieve isotropic uniform growth and avoid the formation of one-dimensional materials[6]. Therefore, increasing the proportion of 2-methylimidazole can make the ZIF-8 particles more uniform. After comprehensive consideration, this experiment determined the optimal ratio conditions for the synthesis of ZIF-8, which is the molar ratio of zinc nitrate hexahydrate to 2-methylimidazole of 1:70 (molar ratio).

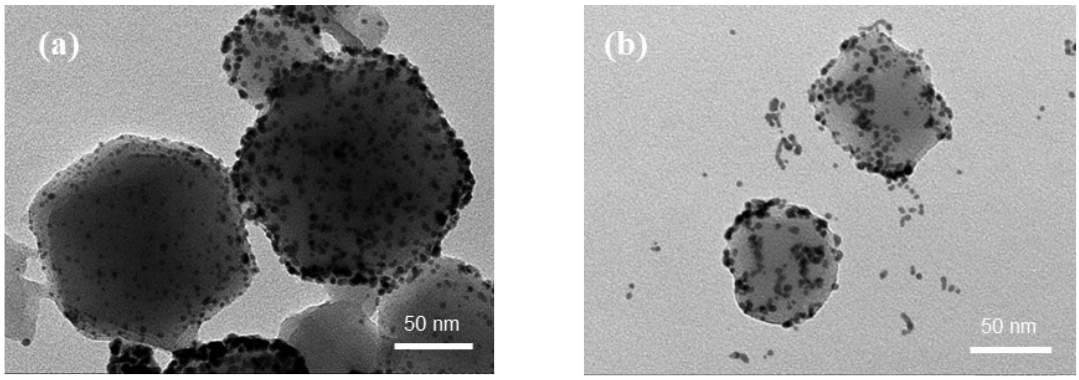

Figure S3 TEM images of Au@ZIF-8 prepared with different amounts of sodium borohydride. (a)200 μL. (b) 400 μL.

The influence of different amounts of reducing agents on Au@ZIF-8.

The size parameters (size and dispersion degree) of Au nanoparticles have a significant impact on the reaction. For gold-based catalysts, it is generally believed that the reduction of Au size is related to the increase in the surface free energy of the active center, which is a favorable condition for the initiation and progress of the reaction. The TEM image of Au@ZIF-8 is shown in **Figure S3**. From the figure, we can clearly observe that in **Figure S3a**, the particle size of Au nanoparticles is mainly 4-5 nm, and they are highly dispersed on the surface of ZIF-8, while the crystal morphology of ZIF-8 remains unchanged; in **Figure S3b**, the particle size of Au nanoparticles is mainly 5-6 nm, and some aggregation phenomena exist, and ZIF-8 changes from the original regular prism structure to a nearly spherical shape. Considering all these factors, the concentration of the reducing agent borohydride sodium added is determined to be 1 mg/mL, and the addition amount is 200 μL.

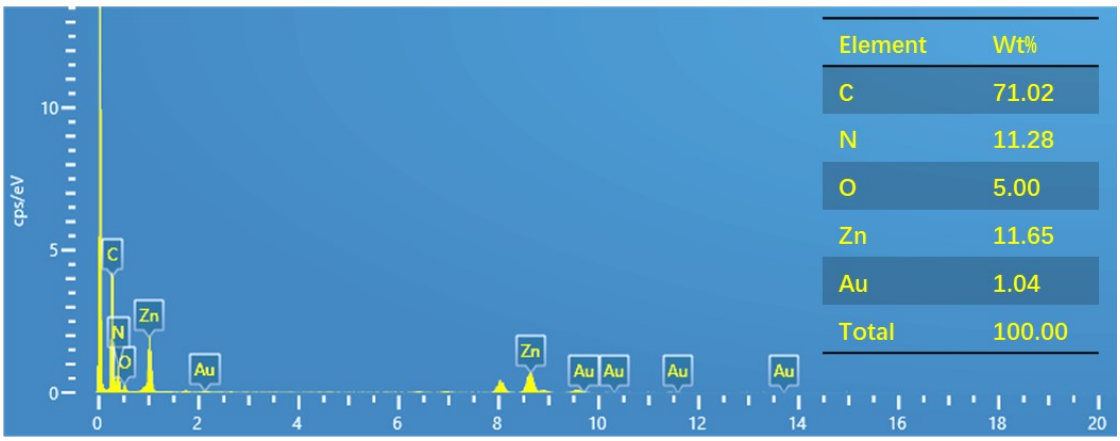

Figure S4 Element distribution of Au@ZIF-8.

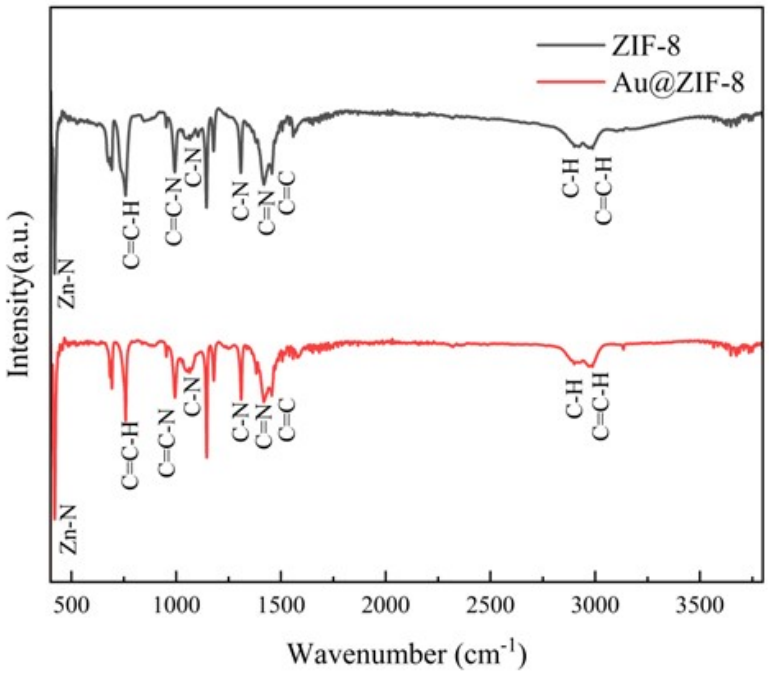

Figure S5 FT-IR spectra of ZIF-8 and Au@ZIF-8 composites.

The FT-IR detection results are shown in Figure S5. 3135 cm^{-1} and 2929 cm^{-1} are the stretching vibration peaks of the methyl and imidazole ring C-H bonds respectively; the main characteristic peaks of the imidazole ring are the stretching vibration of the intramolecular C=C at 1635 cm^{-1}, the stretching vibration of C=N at 1585 cm^{-1}, and the stretching vibrations of C-N at 1438 cm^{-1}, 1308 cm^{-1}, and 1146 cm^{-1}; the main characteristic peaks of the aromatic group are the bending vibration of C-N at 995 cm^{-1} and the bending vibration of C-H at 760 cm^{-1}, and the stretching vibration of Zn-N at 420 cm^{-1} in the ZIF-8 structure; the appearance of these absorption peaks indicates that the ZIF-8 framework has been successfully synthesized[7]. In addition, the characteristic peak of the 2-methylimidazole N-H bond was not detected at 2686 cm^{-1}, which indicates that the ligand has undergone complete deprotonation in this experiment, confirming the acquisition of pure-phase ZIF-8 material[8]. The above results further support that the synthesis scheme determined in this experiment for Au@ZIF-8 material has advantages such as complete ligand conversion, high product purity, and good structural stability.

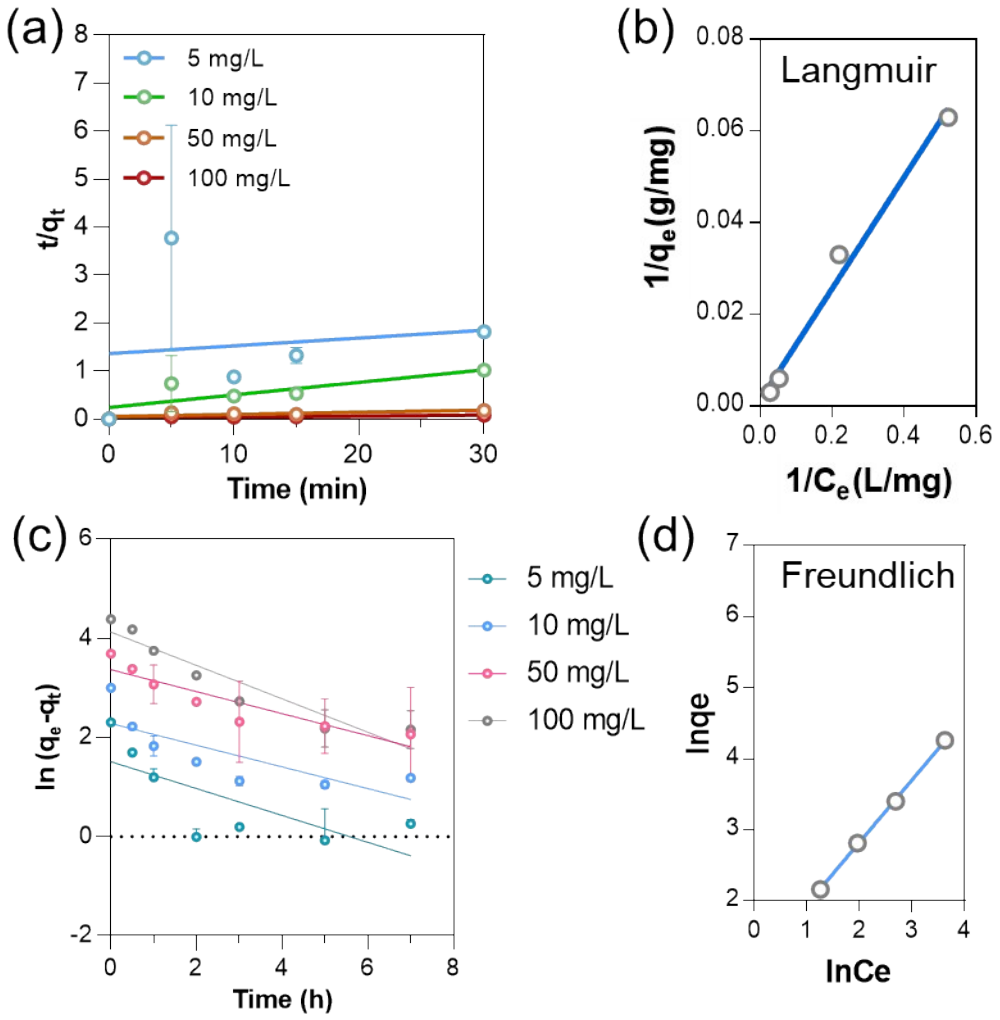

Figure S6 (a) The Pseudo-second-order kinetic model fitting curves for the adsorption of 4-NP by Au@ZIF-8 at different 4-NP concentrations. (b) Au@ZIF-8 adsorption isotherm fitting curve for adsorption 4-NP. (c) The Pseudo-first-order kinetic model fitting curves for the adsorption of NDMA by Au@ZIF-8 at different 4-NP concentrations. (d) Au@ZIF-8 adsorption isotherm fitting curve for adsorption of NDMA.

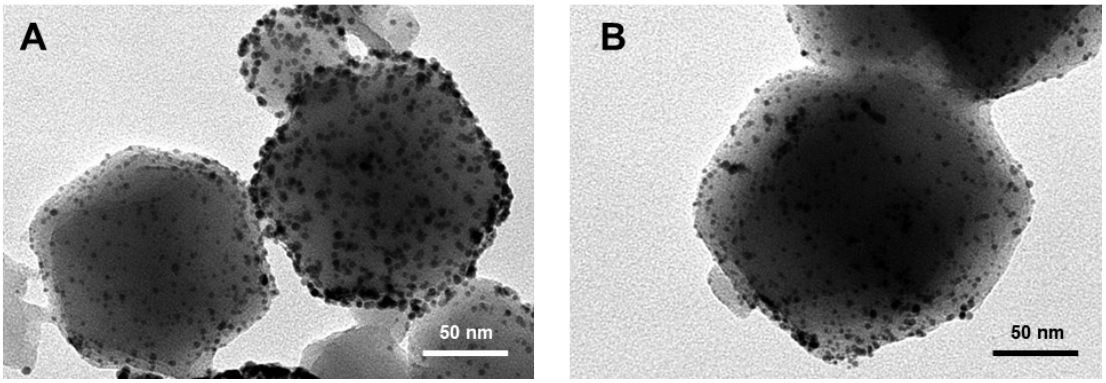

Figure S7 TEM images of Au@ZIF-8 before (A) and after using 10 cycles (B).

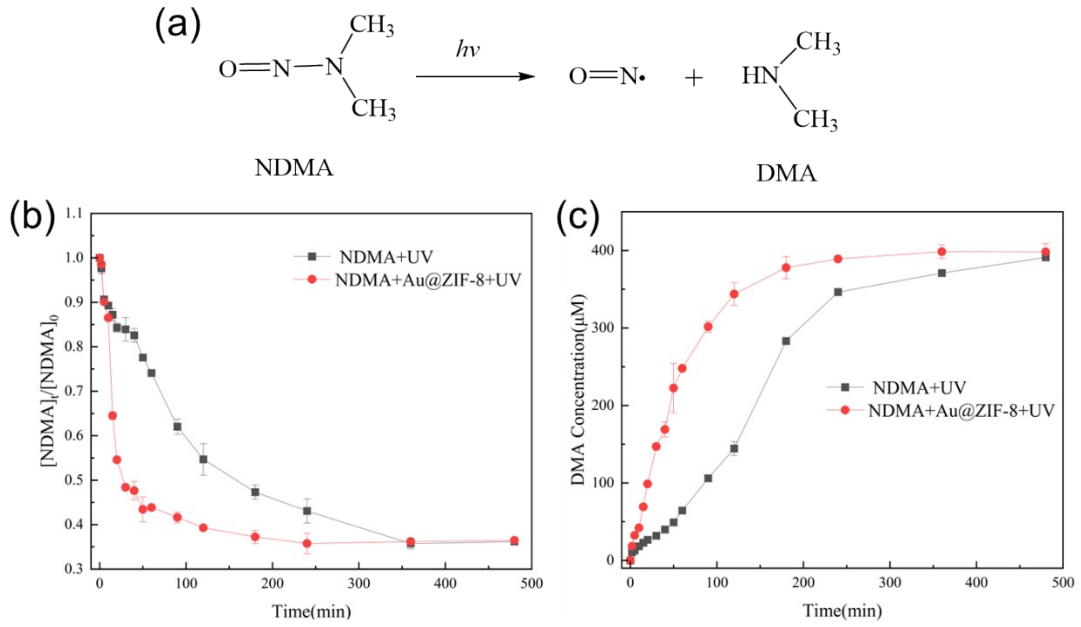

Figure S8 (a) Scheme of photolysis of NDMA. (b) NDMA decomposition time curve under different conditions (*n*=3); (c) Time distribution of NDMA decomposition products DMA under different conditions (*n*=3).

Under ultraviolet light irradiation, the N-N=O bond of the NDMA molecule can be directly photolyzed and broken (**Figure S8a**), generating free radical intermediates, which eventually mineralize into inorganic products[9, 10]. However, this reaction is highly dependent on ultraviolet light, and its efficiency is generally the highest at a short wavelength of 254 nm; moreover, this photodegradation process has a relatively slow reaction rate and is thus limited in practical applications. Therefore, to improve the photodegradation efficiency, oxidants (such as hydrogen peroxide, chlorine gas, etc.) or catalysts (such as titanium dioxide, etc.) are often introduced into the reaction. The results of the 254 nm ultraviolet light photodegradation of NDMA under different conditions are shown in **Figure S8b**. In the presence of Au@ZIF-8, the degradation of NDMA was rapid, reaching a degradation equilibrium in 120 minutes, with a degradation efficiency of approximately 63.5%; while the control group without Au@ZIF-8 had a slow degradation rate, reaching a degradation equilibrium in approximately 360 minutes. Additionally, it has been reported that dimethylamine (DMA) is a product of the ultraviolet light photodegradation of NDMA[11]. Therefore,

DMA was detected using HPLC-MS/MS technology, and the results are shown in **Figure S8c**. In the group with Au@ZIF-8 added, as NDMA decomposed, the product DMA rapidly formed and reached equilibrium at around 180 minutes, with a maximum concentration of 398.17 μM. This indicates that the composite material Au@ZIF-8 has a certain catalytic effect on the photodegradation of NDMA.

Table S1 Specific surface area and pore size properties of ZIF-8 carrier and Au@ZIF-8 composites

Sample	S_{BET} (m^2/g)	S_{micro} (m^2/g)	S_{meso} (m^2/g)	V_{total} (cm^3/g)	V_{micro} (cm^3/g)	V_{meso} (cm^3/g)
ZIF-8	1595.99	1523.68	72.31	0.7758	0.5797	0.1961
Au@ZIF-8	1747.14	1633.13	114.01	0.8175	0.6254	0.1921

Table S2 Au@ZIF-8 adsorption kinetics parameters of 4-NP

concentration/	Pseudo-first-order kinetic model			Pseudo-second-order kinetic model		
(mg/L)	q_e	K_1	R^2	q_e	K_2	R^2
5	20.26	0.05980	0.9469	61.35	0.0039	0.0178
10	33.34	0.04550	0.8233	38.17	0.0101	0.6358
50	191.35	0.08890	0.9530	222.22	0.0003	0.6063
100	393.31	0.08580	0.9652	454.55	0.0001	0.7221

Table S3 Fitting parameters of Au@ZIF-8 adsorption 4-NP adsorption isotherm

Langmuir model			Freundlich model		
q_m	K_L	R^2	n	K_f	R^2
1000.0000	0.0082	0.9862	0.9170	6.9081	0.9923

Table S4 Au@ZIF-8 adsorption kinetics parameters of NDMA

Concentration	Pseudo-first-order kinetic model			Pseudo-second-order kinetic model		
/(mg/L)	q_e	k_1	R^2	q_e	k_2	R^2
5	4.54	0.2643	0.5398	82.65	0.00000	0.9352
10	9.81	0.2189	0.6238	32.15	0.00002	0.9808
20	28.88	0.1910	0.8002	17.33	0.00003	0.9977
50	61.22	0.3285	0.8876	9.12	0.00027	0.9943

Table S5 Fitting parameters of Au@ZIF-8 adsorption NDMA adsorption isotherm

Langmuir model			Freundlich model		
q_m(mg/g)	k_L	R2	n	k_F	R^2
185.1852	0.0140	0.9990	1.1406	2.9247	0.9993

Table S6 Method validation of LC-MS/MS detection method of derivatives DMA from NDMA using Au@ZIF-8.

LOD ($ng \cdot ml^{-1}$)	LOQ ($ng \cdot ml^{-1}$)	Linear Range ($ng \cdot mL^{-1}$)	R^2	RSD% of Repeatability (*n*=6)	RSD% of Stability (24 h)
1	5	5-1000	0.9985	2.77	1.84

Table S7 Comparisons between direct and derivative LC-MS/MS detection for NDMA.

Concentration of NDMA (ng/mL)	Derivative LC-MS/MS detection	Direct LC-MS/MS detection
1	136 (S/N = 6.4)	ND
5	258 (S/N = 13.6)	ND
10	443 (S/N = 33.6)	ND
50	1829 (S/N = 113.6)	ND
100	3074 (S/N = 238.0)	ND
250	7145 (S/N = 754.8)	254 (S/N = 11.7)
500	13033 (S/N = 1353.6)	445 (S/N = 19.2)
1000	27805 (S/N = 2594.9)	961 (S/N = 36.1)

ND indicates not detected.

Table S8 Results of spiked recovery of NDMA in valsartan.

Additon amount (ng/mL)	Peak area	Detection amount (ng/mL)	Recovery (%)	Average (%)	RSD (%)
10	267.98	9.73	97.26		
	268.41	9.74	97.41		
	270.18	9.81	98.05		
20	530.40	19.25	96.25		
	531.20	19.28	96.39	98.18	2.00
	530.50	19.25	96.27		
50	1386.10	50.30	100.61		
	1389.30	50.42	100.84		
	1385.60	50.29	100.57		

References

1. N. M. Mahmoodi, M. Oveisi, A. Taghizadeh and M. Taghizadeh, *Carbohydr. Polym.*, 2020, **227**, 115364.
2. X. Ren, L. Chang, Y. Hu, X. Zhao, S. Xu, Z. Liang, X. Mei and Z. Chen, *Mater. Des.*, 2023, **229**, 111890.
3. G. Kresse and J. Furthmüller, *Phys. Rev. B*, 1996, **54**, 11169-11186.
4. A. Hjorth Larsen, J. Jørgen Mortensen, J. Blomqvist, I. E. Castelli, R. Christensen, M. Dułak, J. Friis, M. N. Groves, B. Hammer, C. Hargus, E. D. Hermes, P. C. Jennings, P. Bjerre Jensen, J. Kermode, J. R. Kitchin, E. Leonhard Kolsbjerg, J. Kubal, K. Kaasbjerg, S. Lysgaard, J. Bergmann Maronsson, T. Maxson, T. Olsen, L. Pastewka, A. Peterson, C. Rostgaard, J. Schiøtz, O. Schütt, M. Strange, K. S. Thygesen, T. Vegge, L. Vilhelmsen, M. Walter, Z. Zeng and K. W. Jacobsen, *J. Phys.: Condens. Matter*, 2017, **29**, 273002.
5. K. Momma and F. Izumi, *J. Appl. Crystallogr.*, 2008, **41**, 653-658.
6. M. Jian, B. Liu, R. Liu, J. Qu, H. Wang and X. Zhang, *RSC Adv.*, 2015, **5**, 48433-48441.
7. J. Liu, J. He, L. Wang, R. Li, P. Chen, X. Rao, L. Deng, L. Rong and J. Lei, *Sci Rep*, 2016, **6**, 23667.
8. K. A. Lin and H. Chang, *Water, Air, & Soil Pollution*, 2015, **226**, 10.
9. H. Sakai, T. Takamatsu, K. Kosaka, N. Kamiko and S. Takizawa, *Chemosphere*, 2012, **89**, 702-707.
10. M. H. Plumlee, M. López-Mesas, A. Heidlberger, K. P. Ishida and M. Reinhard, *Water Res.*, 2008, **42**, 347-355.
11. C. Lee, W. Choi, Y. G. Kim and J. Yoon, *Environ. Sci. Technol.*, 2005, **39**, 2101-2106.